

## Computation of GOAHEAD configuration with Chimera assembly

*T. Renaud\**, *M. Costes\**, *S. Péron\*\**

\* ONERA, 8 rue des Vertugadins, 92190 Meudon, France

Email address: [thomas.renaud@onera.fr](mailto:thomas.renaud@onera.fr)

Phone number: (33) 1 46 73 42 40

Fax number: (33) 1 46 73 41 46

\*\* ONERA, BP 72, 29 Avenue de la Division Leclerc, 92322 Châtillon, France

### Abstract

In the framework of the GOAHEAD European project, CFD simulations around a complete helicopter configuration have been performed by the different partners to validate their codes and to compare with a detailed experimental database. At ONERA, the simulation of such a complex configuration is still challenging in terms of efforts required in the pre-processing phase, and in terms of CPU time. This test-case has been in particular used to set up a pre-processing chain of tools, going from the meshes described in a CGNS tree to the calculation input. This chain including the Chimera assembly of the different components of the helicopter is described in this paper. The second part presents some results of one of the test-cases performed by ONERA in the project: the cruise/tail shake flight condition. The results are compared with the experiment data and also with pre-tests CFD computations.

## 1 INTRODUCTION

Helicopter aerodynamics is a particularly difficult problem because it combines the effects of unsteady transonic flows on the advancing side of the main rotor blades, low-speed high angle of attack conditions on the retreating blade side, which may lead to dynamic stall, low-speed flows around the fuselage and the rotor head with significant parts of flow separation and thick unsteady wakes, and large wake interactions due to a combination of the low-speed flight conditions and of the blades rotation. An additional difficulty results from the strong interactions, which are inherent to helicopters' architecture, between the blades aerodynamics and dynamics, due to the articulated hub which is required for the mechanical aspect of the rotor. As a result, the blade motion and deformation have to be determined for any flight condition. Finally, helicopters operate at very different conditions even during a single mission profile, so that many very different flight conditions are important and have to be considered.

The simulation of complete helicopter configurations by numerical methods is therefore one order of magnitude more complex than its fixed wing counterpart, and the level of maturity of CFD for rotorcraft applications always lagged behind that of most other ones in the aeronautical field. Indeed, the helicopter has been perceived as a good candidate for developing and assessing new numerical techniques, e.g. in order to be capable to describe various sets of bodies in relative motion. Basically, CFD techniques began to come to maturity for complete helicopter applications in the decade 1995-2005. Recent applications were shown e.g. in [1], [2], [3].

At ONERA, the development of CFD techniques for complete helicopter applications was achieved within the CHANCE project, performed in close cooperation with DLR, Eurocopter, Eurocopter Deutschland and IAG (University of Stuttgart) [4]. Nevertheless, it was clear before the end of the project that a detailed validation of such heavy numerical simulations lacked of well-documented experimental data. As a matter of fact, the

complexity of the helicopter directly impacts that of wind-tunnel testing, and therefore wind-tunnel testing of complete helicopter configurations for highly instrumented models is not only very difficult to perform but also very expensive. This lack of database motivated most of the European helicopter research and industry community to join their effort and launch the GOAHEAD project [5]. This project essentially aimed at testing a fully instrumented complete helicopter model in the LLF facility of the DNW. In parallel to that, CFD simulations were completed by the partners before and after the conduction of the wind-tunnel tests, and compared with experimental data. The objective of this paper is to present the numerical contribution of ONERA in the project.

## 2 EXPERIMENT DESCRIPTION

The model tested in GOAHEAD was made of existing components, including the 7AD 4-bladed main rotor, a NH-90 fuselage and a 2-bladed Bo-105 tail rotor models. Both main and tail rotors were equipped with unsteady pressure transducers and strain gauges. Adaptation of the various components was required, more especially for the integration of the tail rotor into the fuselage and the instrumentation of the fuselage. Additionally, a fairing for the rotor head had to be manufactured. Other measurement devices included hot films on the fuselage and the main rotor blades, PIV in several regions of interest around the model, SPR optical measurement of the main rotor blades deflection complementary to the SPA procedure from the strain gauges, infrared thermography for the laminar-turbulent transition and 6-component balances.

Four different test-points were defined in common by the partners, with corresponding test conditions for the isolated fuselage as well. They aimed at covering important flight conditions of the helicopter, namely low-speed pitch-up, cruise/tail shake, high-loaded high-speed and very high-speed cases. ONERA was in charge of computing two of them, the cruise/tail shake condition and the

very high-speed case but this paper focuses on the first one. The control angles were coming from a HOST rotor trim (HOST is the Eurocopter comprehensive code for the flight mechanics of the helicopter). For the cruise/tail shake test case, the Mach number is  $M_\infty=0.204$ , fuselage pitch  $\alpha=-2.5^\circ$ , tip Mach number of the main rotor  $M_{Tip\_MR}=0.617$  and tip Mach number of the tail rotor  $M_{Tip\_TR}=0.563$ .

## 3 NUMERICAL METHODS

### 3.1 Description of the flow solver

The simulation has been performed using *elsA* structured CFD solver, developed at ONERA. The 3D compressible RANS equations are solved by a Finite-Volume cell-centred approach for both off-body Cartesian and near-body curvilinear grids.

The spatial discretisation of the governing equations is achieved by a 2<sup>nd</sup>-order Jameson scheme, with a 2<sup>nd</sup> and 4<sup>th</sup>-order artificial dissipation ( $k_2=0.5$ ,  $k_4=0.016$ ). The time integration is performed by a Backward Euler scheme, with 10 Gear subiterations. No low-Mach preconditioning has been applied in that study, and 2<sup>nd</sup> order Chimera interpolations have been used to transfer the solution between overlapping grids. Kok's two-equation  $k-\omega$  model is used to model the turbulence. The wind tunnel walls are modeled by inviscid wall boundary conditions, whereas the walls of the other components (fuselage, strut, main and tail rotor) are modeled by no-slip boundary conditions.

The simulation starts from a non-disturbed free-stream initial condition. The first main rotor revolution has been completed using a constant time step, corresponding to a variation of 3 degrees of azimuth; then, five rotor revolutions are computed using a time step corresponding to a variation of 1 degree of azimuth. On 8 Montecito Intel Itanium processors, a main rotor revolution required about 7 days CPU.

### 3.2 Description of the mesh

The mesh is composed by a set of structured near-body grids describing each component of the configuration, that are the fuselage, the hub, the strut, the main rotor blades, the tail rotor blades, the wind tunnel walls, and by a set of off-body Cartesian grids.

Each component is meshed independently, which enables to add or remove a feature on the configuration easily, such as the hub. Then the Chimera assembly ensures the coupling between solutions defined on all the grids.

The fuselage, strut, and hub meshes are composed respectively by 7.4, 1.3 and 1.1 million points. There are 1.4 million points describing the wind tunnel walls, 1.1 million points for each blade of the main rotor, and 0.65 million points for each blade of the tail rotor.

The off-body grids are automatically generated given the set of near-body grids, thanks to a mesh generation external python module. The off-body mesh consists in a set of overset regular Cartesian grids describing the whole computational domain, and which overlap the near-body grids [6][7]. Different levels of refinement are performed, with the finest grids located in the vicinity of the bodies. The spatial step on Cartesian grids of the finest levels are determined by a mean of the size of the cells located at the external borders of near-body grids, in order to perform Chimera transfers between near-body and off-body grids with an interpolation error corresponding to the error of the numerical scheme. The Cartesian off-body mesh is composed by 12.3 million points distributed over 251 blocks. All the data of the resulting Cartesian mesh, including the physical boundary conditions and the overlap boundary conditions, are provided as a basis of the CGNS tree containing the information of the near-body meshes. A view of the resulting mesh is presented in Figure 1: each body is meshed by a shortly-extended set of curvilinear grids (in green for the strut, red for the fuselage, dark blue for the hub, pink for

the main rotor, and light blue for the wind tunnel walls). Cartesian off-body grids (in black) are finer near the helicopter and coarser elsewhere.

### 3.3 Chimera assembly

The Chimera method has been developed at ONERA for many years in the *elsA* solver for CFD simulations of helicopter configurations [8]. Two Chimera assembly approaches have been considered here, depending if the two bodies considered are in relative motion or not. In the first case, the Chimera hole-cutting is performed into the solver at each iteration, whereas in the other case, the Chimera assembly is performed using a Chimera connectivity pre-processing tool, called Connector [9], described below. In both cases, cells lying in a body at any time must be blanked.

First, since the main and tail rotor blades are in motion at each iteration of the simulation, then the Chimera blanking involving these components must be performed at each iteration. Blade surfaces are not in contact with another component, so the blanking can be performed using these surfaces by the X-Ray hole-cutting technique developed by Meakin [10]. Thus blanked cells of the fuselage, hub or Cartesian off-body grids due to each blade are determined at each iteration.

For the fuselage, strut and hub components, the Chimera hole-cutting has been performed in a pre-processing stage using the Connector module, which is a CGNS-based python module. It includes several features such as X-Ray hole-cutting, overlap optimization, and simplifies the setting up of the Chimera assembly. One advantage of the X-Ray hole-cutting technique in Connector, compared to the one in the solver is that the body that defines the X-Ray solid object does not have to be a wall boundary defined in the computation.

Another feature of Connector is a so-called inverted X-Ray hole-cutting technique,

in order to blank cells out of a solid. This inverted technique has been used to blank Cartesian grid cells lying out of the wind tunnel walls, which bound the computational domain, as shown in Figure 2. Figure 3 represents the result of the inverted X-Ray blanking near the wind tunnel walls, with an extension determined to get a small overlapping between wind tunnel grids and Cartesian grids.

Here, given the different components, whose mesh are defined as a basis of the python CGNS tree, and considering a relationship between each component (e.g. an union to add the strut onto the fuselage), blanking is automatically done. For instance, the Cartesian grids are blanked by the fuselage, hub, strut and wind tunnel walls. In Figure 1 is presented a detailed view of the mesh around the hub after blanking with Connector (no overlap optimization has been performed here).

## 4 CRUISE TEST-CASE

### 4.1 Field data

First of all, Figure 4 presents the complexity of the flowfield simulated around the complete helicopter. On the retreating side (right part of the helicopter), the rotor wakes is highlighted through an isosurface of  $Q$  criteria colored by vorticity. The interactions between both rotors together and with the fuselage are important and can be detected by the isocontours of pressure coefficient on the advancing side (left part of the helicopter). The main rotor tip vortices impact the nose and the fin of the fuselage. The rotating main rotor hub leads also to the convection of unsteady turbulent structures downstream.

It can also be noticed that despite the use of automatically generated Cartesian background grids, the vortices are rapidly diffused as the Cartesian mesh is not adapted during the rotor revolution. Nevertheless, the main flow characteristics are well captured.

### 4.2 Loads data

After the previous qualitative look at the flowfield, some quantitative results are presented below.

At first, the loads (drag, side and lift forces coefficients) of the helicopter fuselage and the main rotor are shown respectively in Figure 5 and Figure 6. Even if they are not fully comparable (in particular in terms of forces) due to different geometries and control angles, the blind test (dashed lines) and post test (solid lines) are put on the same graphs. It should also be added here that the blind test were run on a common grid shared by the partners and generated by DLR, contrary to the post-test computations which were run using grids generated in common with Eurocopter. The 4/rev periodicity resulting from the four blades passage is quite well captured on the fuselage and the main rotor and shows the correct time-convergence of the computation to a periodic solution. Note that the convergence of the post test calculations has been improved as a consequence of the better grid quality.

### 4.3 Pressure data

In Figure 7, steady and unsteady experimental pressure data are plotted with symbols over the computed isocontours of pressure coefficient  $C_p$  at main rotor azimuth  $\psi=60^\circ$ . The numerical results are in good agreement with experiment, in particular on the rear part of the fuselage (horizontal stabilizer and vertical fin) where the interactions with the rotor wakes are well simulated.

The next figure presents some examples of unsteady pressure sensor data during a main rotor revolution; their positions on the fuselage are also shown in Figure 8. The results are plotted in black for the experiment, in blue for the preliminary blind test computations and in red for the post test solutions. The 4/rev periodicity is clear for the transducers A06 and A20, as the main rotor wake impacts directly the nose of the

fuselage. Thus, there is a good agreement between both calculations and experiment. The following three sensors K22, K23 and K24 are located in the “doghouse” where structures coming from the strut interact with the flow separation along the backdoor ramp. The influence of the main rotor is no more visible in that area, except the asymmetry between K23 and K24 data due to the rotor downwash. This asymmetry is well reproduced with the new simulations, as the better mesh resolution allows keeping the flow features from the main rotor to the lower part of the fuselage. The K57 and K58 sensors are located on both sides of the vertical fin. The K58 transducer is directly impacted by the tail rotor flow and delivers a 10/rev periodic signal (the two blades of the tail rotor rotate five times faster than the four-bladed main rotor). However, both CFD computations overestimate the amplitude of the pressure oscillations. On the other side (K57 sensor), the 4/rev periodicity is still predominant and the post test results are in better agreement with experiment than the blind test ones.

Figure 9 and Figure 10 present the distribution of sectional surface pressure data  $C_p M^2$  for the main rotor, respectively for the advancing and retreating sides. The post test computations (in solid lines) are compared to the blind test (in dashed lines) and experimental (red symbols) results. The sectional surface pressure data on the main rotor blade are in qualitatively correct agreement with the experimental values. With respect to the blind test results, the post test computations improved slightly the negative peak of  $C_p M^2$  at the leading edge and did not show this strange separation at  $r/R=0.5$  and  $r/R=0.7$ , due to a better boundary layer resolution.

## 5 CONCLUSIONS AND PERSPECTIVES

The GOAHEAD project was a good opportunity for a large number of partners from the rotorcraft community in Europe to

develop and evaluate their aerodynamic simulation capabilities for complete helicopter configurations. At ONERA, the effort aimed at making these complex numerical simulations more straightforward in order to facilitate their use in the design office, based on the CGNS data structure and an automatic setting of the Chimera framework capable to deal with general and multiple body positioning and motion, including the generation of the Cartesian background grid, hole cutting and Chimera interpolation. This allowed running the simulations using common grids generated by another partner as well as in-house generated grids. Comparison with experimental data shows that the simulations correctly predict the flow physics, although a too large wake diffusion leads to a degradation of the quality of the solution in the rear part of the helicopter.

Future activities will concern an adaptation of the Cartesian background grid to the wake solution, together with the use of improved wake-conservation schemes, as well as the coupling of the CFD simulation with HOST dynamics and trim.

## 6 ACKNOWLEDGEMENTS

The present work has been partially funded by the European Union under the Integrating and strengthening the European Research Area Programme of the 6<sup>th</sup> Framework, Contract Nr. 5160714.

## 7 REFERENCES

- [1] M. Bhagwat, A. Dimanlig, H. Saberi, E. Meadowcroft, B. Panda, R. Strawn, *CFD/CSD Coupled Trim Solution for the Dual-Rotor CH-47 Helicopter Including Fuselage Modeling*, AHS Specialists' Conference on Aeromechanics, San Francisco, CA, January 2008.
- [2] W. Khier, *Numerical simulation of air flow past a full helicopter configuration*, 35<sup>th</sup> European Rotorcraft Forum, Hamburg, Germany, September 2009.

- [3] M. Potsdam, M. Smith, T. Renaud, *Unsteady computations of rotor-fuselage interactions*, 35<sup>th</sup> European Rotorcraft Forum, Hamburg, Germany, September 2009.
- [4] T. Renaud, A. Le Pape, C. Benoit, *Unsteady Euler and Navier-Stokes computations of a complete helicopter*, 31<sup>st</sup> European Rotorcraft Forum, Florence, Italy, September 2005.
- [5] M. Raffel, F. de Gregorio, W. Sheng, G. Gibertini, A. Seraudie, K. de Groot, B. van der Wall, *Generation of an advanced helicopter experimental aerodynamic database*, 35<sup>th</sup> European Rotorcraft Forum, Hamburg, Germany, September 2009.
- [6] R.L. Meakin, *Adaptive Spatial Partitioning and Refinement for Overset Structured Grids*, Computer Methods in Applied Mechanics and Engineering, vol. 189, pp. 1077-1117, 2000.
- [7] C. Benoit, G. Jeanfaivre, *Three-dimensional inviscid isolated rotor calculations using Chimera and automatic Cartesian partitioning methods*, Journal of the American Helicopter Society, 48:22, pp. 128-138, 2003.
- [8] C. Benoit, G. Jeanfaivre, E. Canonne, *Synthesis of ONERA Chimera method developed in the frame of CHANCE programme*, 31<sup>st</sup> ERF, 2005.
- [9] S. Péron, C. Benoit, P. Raud, *Développement de techniques de pré-traitement Chimère pour la prise en compte de détails technologiques dans les turbomachines*, RT4/14231 DSNA, ONERA Technical report, 2010.
- [10] R.L. Meakin, *Object X-Rays for Cutting Holes in Composite Overset Structured Grids*, AIAA Paper 2001-2537, 2001.

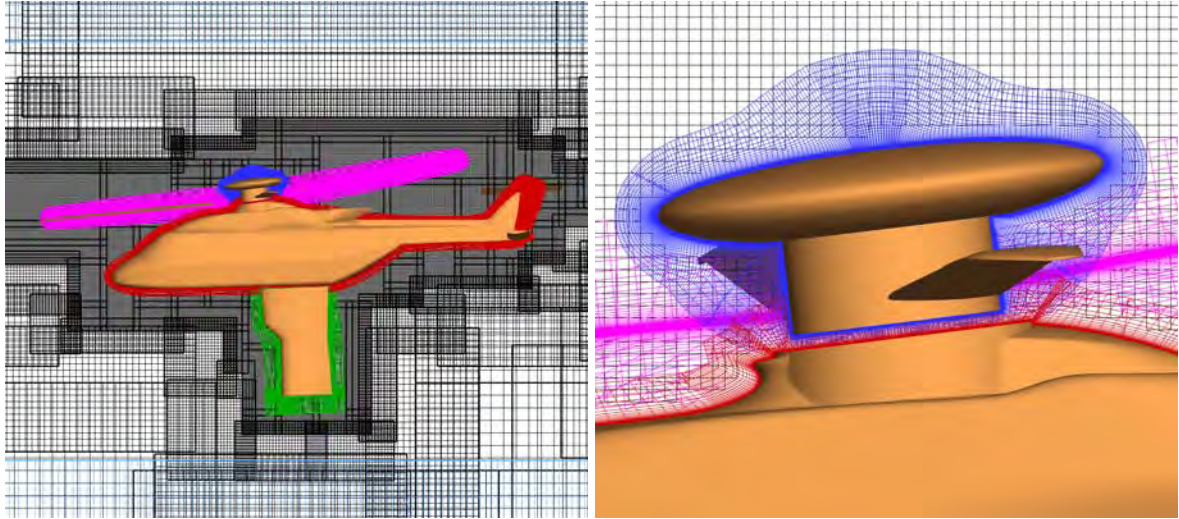


Figure 1 - Close-up view of the global mesh (left) and of the Chimera blanking near the hub (right)

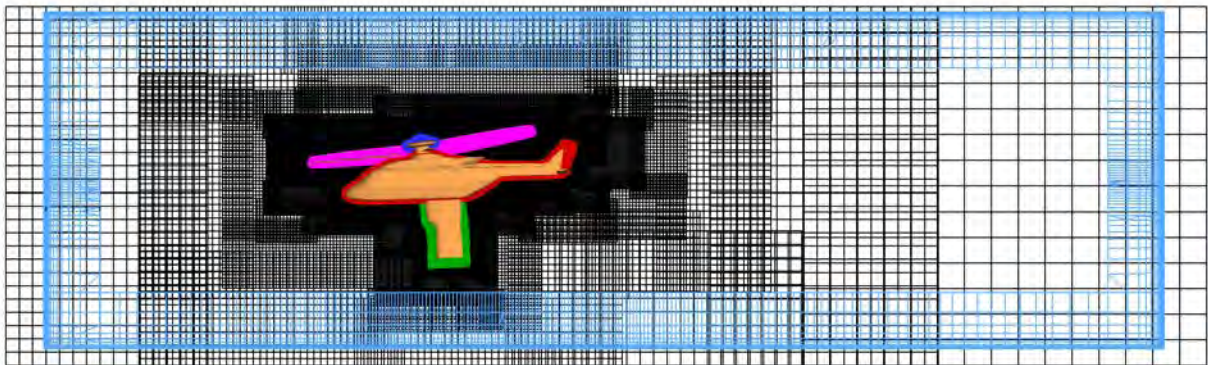


Figure 2 - Cartesian off-body grids extension out of the wind tunnel walls

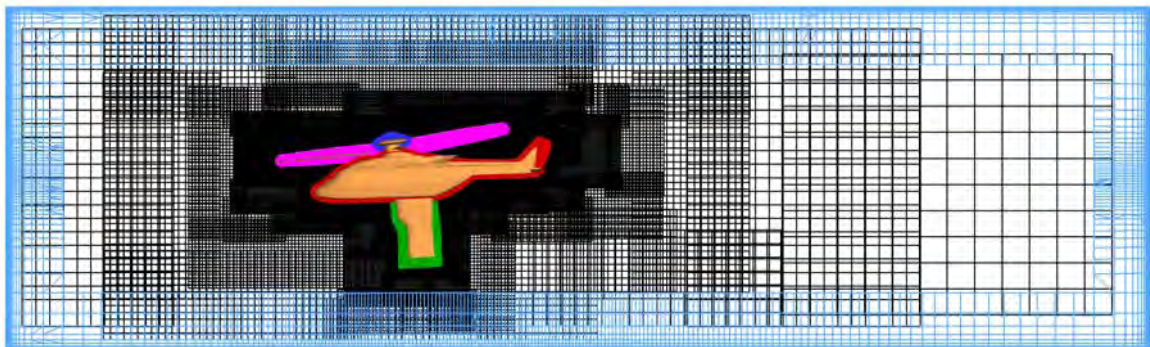


Figure 3 - Result of the inverted hole-cutting near the external boundaries

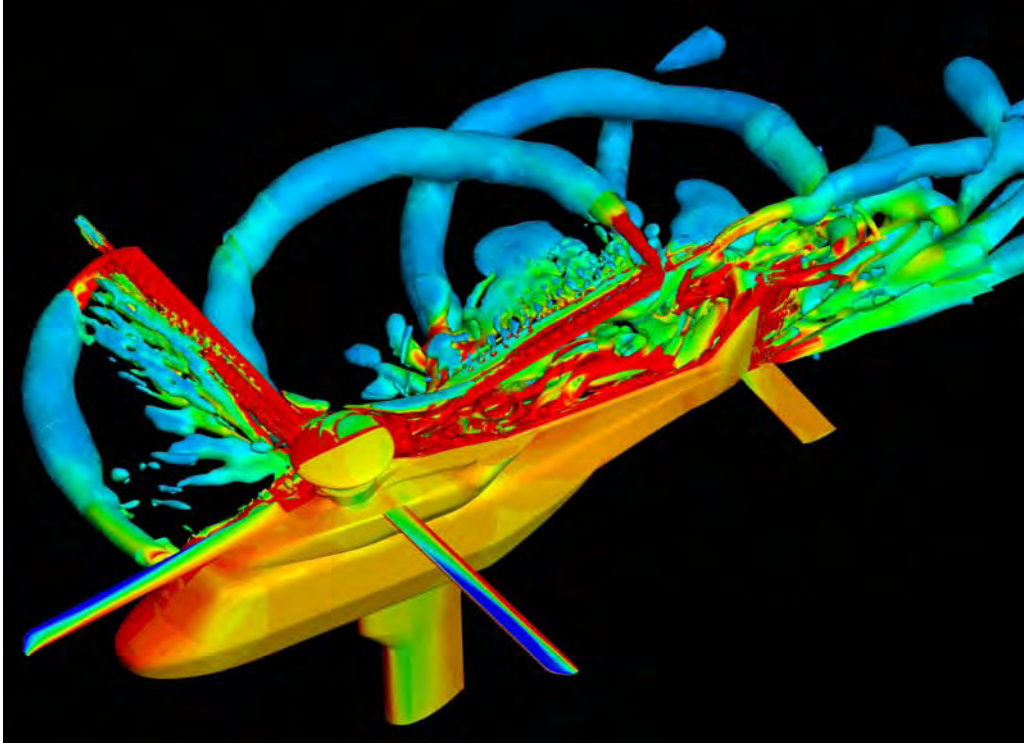


Figure 4 - Colored view of the flow solution around the GOAHEAD configuration (pressure coefficient on wall surfaces and wakes represented by isosurface of Q criteria)

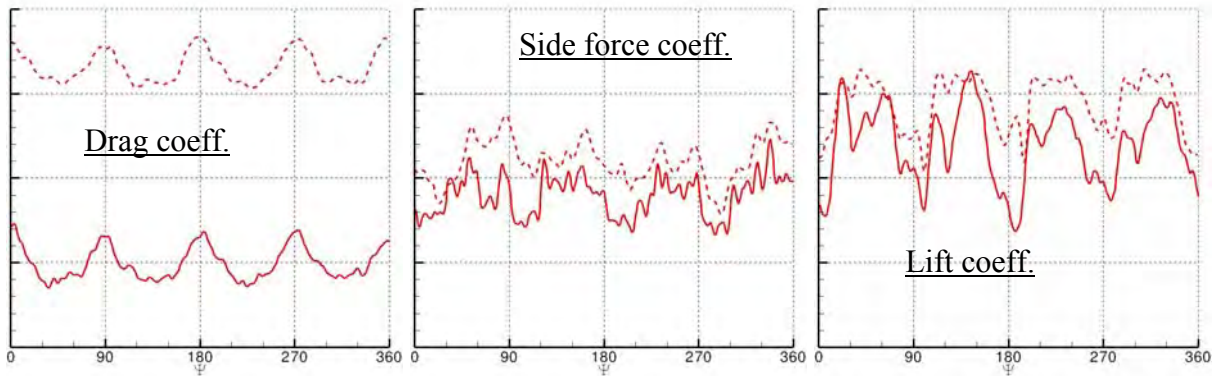


Figure 5 - Force data of the helicopter fuselage for the cruise and high-speed tail-shake test case (dashed line = blind test, solid line = post test)

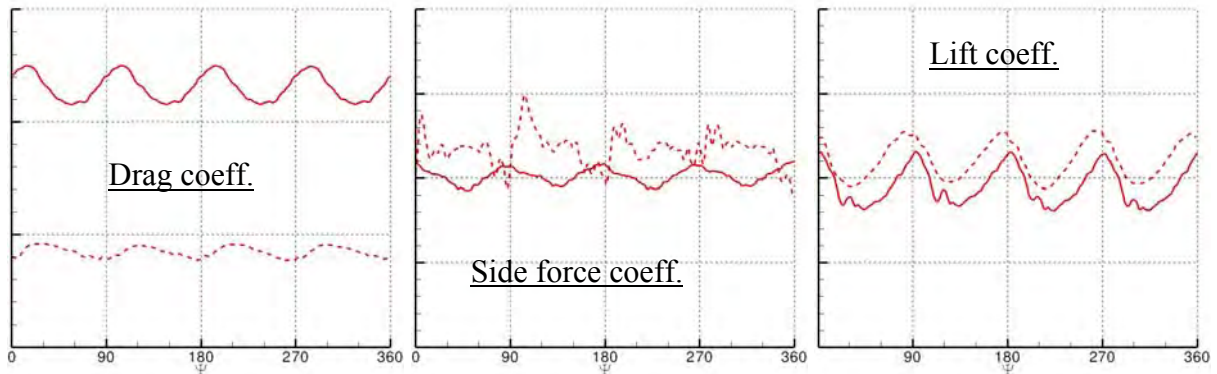


Figure 6 - Force data of the main rotor for the cruise and high-speed tail-shake test case (dashed line = blind test, solid line = post test)

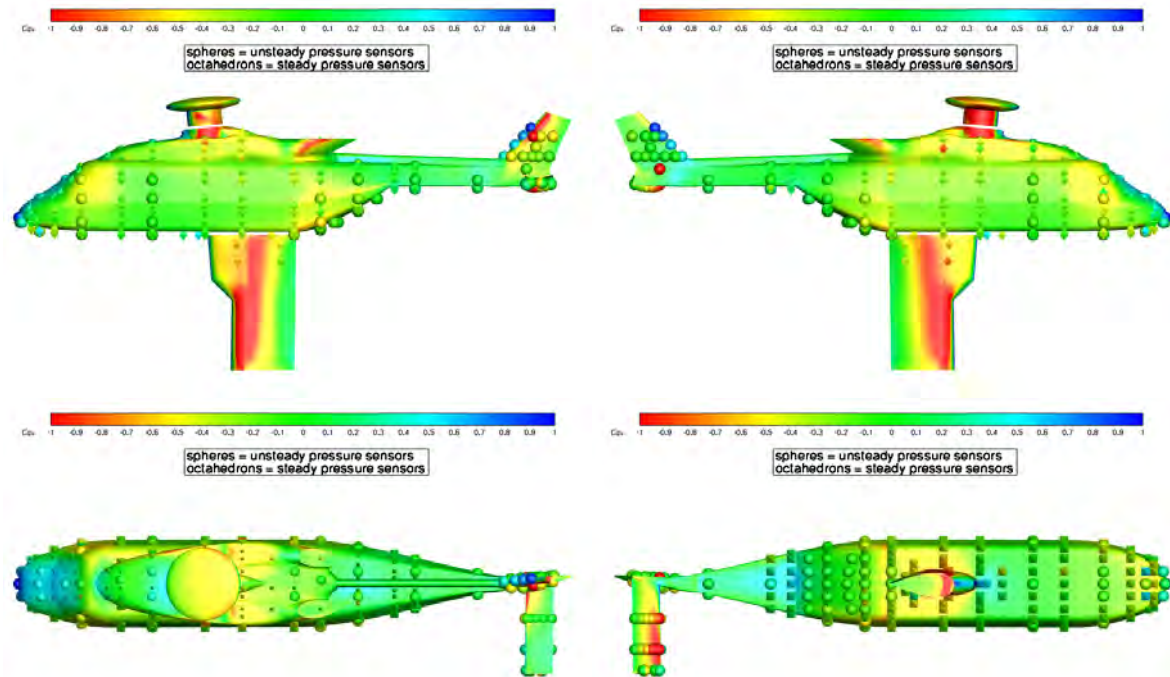


Figure 7 - Surface pressure coefficient  $C_p$  for the cruise and high-speed tail-shake test case at main rotor azimuth  $\psi=60^\circ$

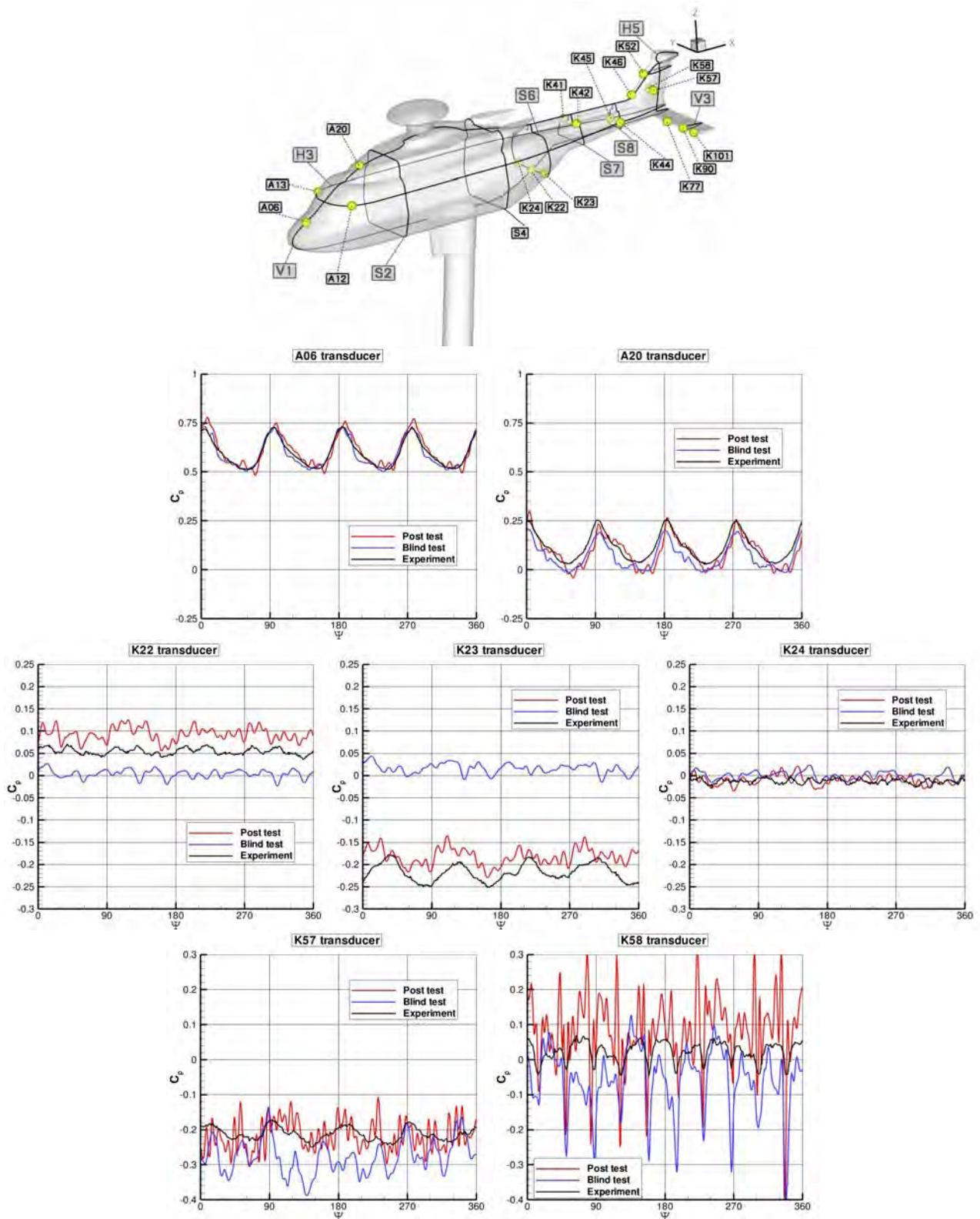


Figure 8 - Location and results of pressure sensor data ( $C_p$ ) for the cruise and high-speed tail-shake test case (black line = experiment, blue line = blind test, red line = post test)

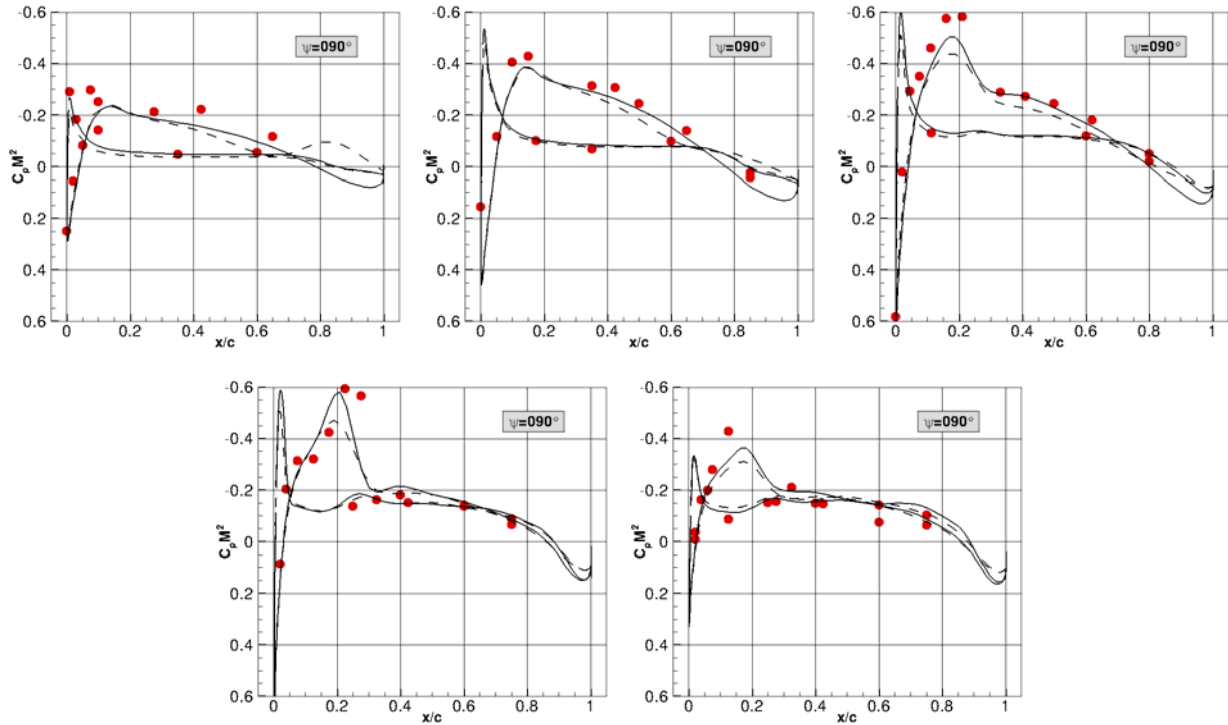


Figure 9 - Sectional surface pressure data ( $C_p M^2$ ) for the main rotor at advancing side for the cruise and high-speed tail-shake test case. Solutions are shown at  $r/R=0.5 - 0.7 - 0.825 - 0.915 - 0.975$  section position on the blade (dashed line = blind test, solid line = post test)

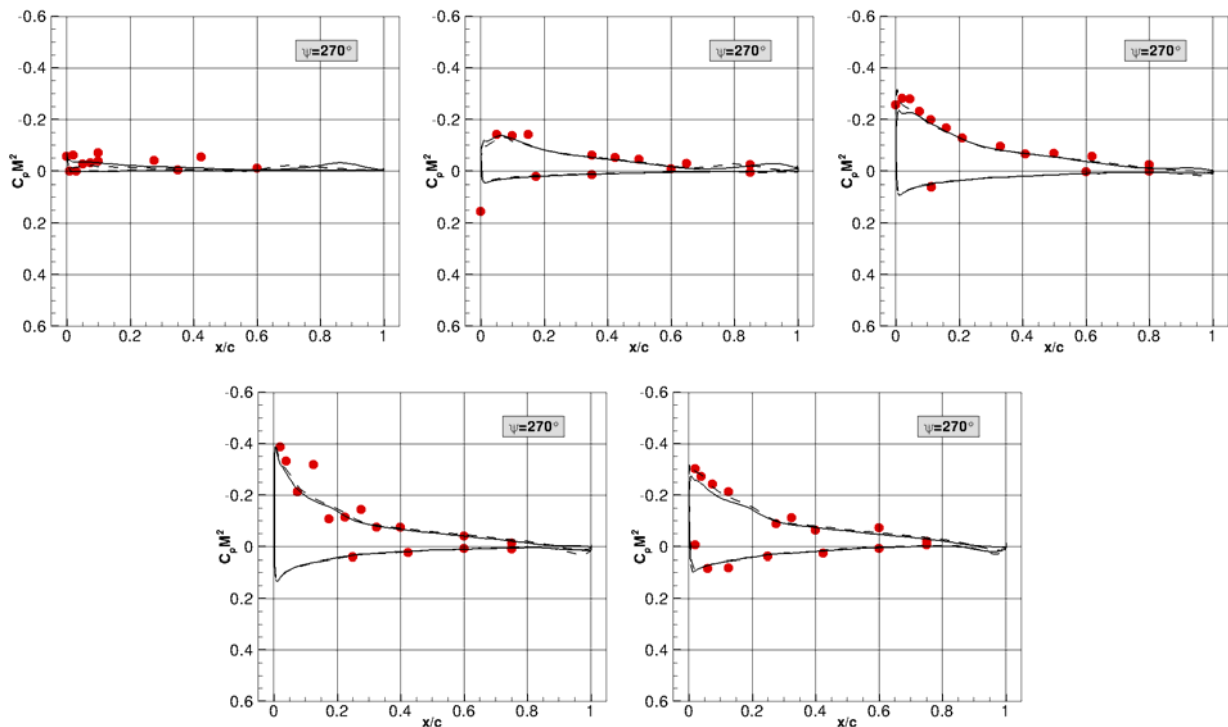


Figure 10 - Sectional surface pressure data ( $C_p M^2$ ) for the main rotor at retreating side for the cruise and high-speed tail-shake test case. Solutions are shown at  $r/R=0.5 - 0.7 - 0.825 - 0.915 - 0.975$  section position on the blade (dashed line = blind test, solid line = post test)